Coke Formation in a Zeolite Crystal During the Methanol-to-Hydrocarbons Reaction as Studied with Atom Probe Tomography

Joel E. Schmidt, Jonathan D. Poplawsky, Baishakhi Mazumder, Özgün Attila, Donglong Fu, D. A. Matthijs de Winter, Florian Meirer, Simon R. Bare,* and Bert M. Weckhuysen*

Abstract: *Understanding the formation of carbon deposits in zeolites is vital to developing new, superior materials for various applications, including oil and gas conversion processes. Herein, atom probe tomography (APT) has been used to spatially resolve the 3D compositional changes at the sub-nm length scale in a single zeolite ZSM-5 crystal, which has been partially deactivated by the methanol-to-hydrocarbons reaction using ^{13}C-labeled methanol. The results reveal the formation of coke in agglomerates that span length scales from tens of nanometers to atomic clusters with a median size of 30–60 ^{13}C atoms. These clusters correlate with local increases in Brønsted acid site density, demonstrating that the formation of the first deactivating coke precursor molecules occurs in nanoscopic regions enriched in aluminum. This nanoscale correlation underscores the importance of carefully engineering materials to suppress detrimental coke formation.*

Zeolites are crystalline, microporous materials that exhibit robust hydrothermal stability, allowing them to be used under demanding process conditions, such as oil refinery operations[1,2] and automotive emissions treatments.[3,4] Commercially, one of the most important zeolites is ZSM-5 with MFI framework topology, which has become ubiquitous in petroleum refining and chemical manufacturing.[2] The enormous

quantities at which this material is utilized at the global scale continue to drive research targeting improved performance. The detrimental formation of coke is one of the factors limiting zeolite materials, particularly ZSM-5, in high-demand catalytic processes, such as fluid catalytic cracking (FCC) and the methanol-to-hydrocarbons (MTH) reaction.

ZSM-5 coking in the MTH reaction has long been studied, with a range of conclusions regarding the nature and mechanism of coke formation.[5,6] Despite ongoing investigations and debates, there is a consensus that coking occurs due to the formation of alkylated mono- and polycyclic aromatics near internal channel intersections, followed by an increase in surface coke from polycyclic arenes near pore openings, which finally form a graphitic layer and block pore access.[7–13] In order to more fully elucidate the material properties that promote the detrimental formation of coke during the MTH reaction on ZSM-5, it would be beneficial to study the carbon deposits on the sub-nm length scale. Previous coking studies on ZSM-5 in the MTH reaction have concentrated on the bulk,[7–9,13] or on micrometer length scales,[10,11,14,15] to gain some spatial insight, but none have been capable of delivering sub-nm resolution.

The only characterization method currently capable of spatially resolving 3D element distributions at the sub-nm scale is atom probe tomography (APT), which was first envisioned in the 1930s, but has recently experienced rapid growth due to improvements in instrumentation.[16–20] APT is able to create atom-by-atom 3D compositional reconstructions of materials within a fabricated needle-shaped specimen (tens of nanometers in size), across which a high electric field is applied that causes atoms to evaporate during pulsing events. The ions are then spatially detected and their identity determined using time-of-flight mass spectrometry. This technique has traditionally been used to study conductive materials,[19] but owing to experimental advances, APT can also now be applied to non-conductive materials. APT was recently applied to zeolites for the first time to study the distribution of Al atoms in parent and severely steamed, large, coffin-shaped ZSM-5 crystals, where a non-uniform Al distribution was observed.[21]

Herein, we report the use of APT to create 3D compositional reconstructions with sub-nm resolution of a ZSM-5 crystal that has been used in the MTH reaction. The aim of the study was to determine the impact of the reaction on the distribution of framework atoms, as well as to study the distribution of coke within the ZSM-5 crystal. The MTH reaction was performed using ^{13}C-labelled methanol so that coke species could be unambiguously assigned, with a 90 min reaction time at 623 K purposefully chosen to yield crystals

[*] Dr. J. E. Schmidt, Ö. Attila, D. Fu, Dr. F. Meirer,
Prof. Dr. B. M. Weckhuysen
Debye Institute for Nanomaterials Science
Utrecht University
Universiteitsweg 99, 3584 CG Utrecht (The Netherlands)
E-mail: b.m.weckhuysen@uu.nl
Homepage: http://www.anorg.chem.uu.nl

Dr. J. D. Poplawsky, B. Mazumder
Center for Nanophase Materials Sciences, Oak Ridge National Laboratory
Oak Ridge, TN 37831 (USA)

Dr. D. A. M. de Winter
Structural Geology & EM, Utrecht University
Postbus 80.021, 3508 TA Utrecht (The Netherlands)

Dr. S. R. Bare
SLAC National Accelerator Laboratory
2575 Sand Hill Road
Menlo Park, CA 94025 (USA)
E-mail: simon.bare@slac.stanford.edu

that contained sufficient coke for analysis, while still retaining catalytic activity (see Figure S1 and the Supporting Information for further explanation).[13,14] Using advanced cluster analysis we provide an atomic scale visualization of hydrocarbon deposits within a single ZSM-5 crystal, and demonstrate a correlation between the Brønsted acid site density on a nanoscopic level and the formation of ^{13}C clusters (the term cluster refers to a group of closely positioned atoms).

The ZSM-5 crystals employed in this work contain a complex internal architecture, shown in Figure 1a.[22] For APT analysis a cross-section of the ZSM-5 crystal used in the MTH reaction was prepared via focused ion beam (FIB) milling from a portion of the crystal that contained several different subunits. The locations of the cross-section and needles prepared for APT are shown in Figures 1b and S2, and images of all analyzed needles are displayed in Figure S3. In total four needles were successfully analyzed by the APT technique (see the Supporting Information for details about the APT experiment and related data analysis). Within the material, internal diffusion barriers exist between subunits (Figure 1a) and the composition (Si/Al ratio) of the material is clearly non-uniform (Figure 1c).[22] The ZSM-5 crystal

exhibits a silica-rich crust region that forms the first 10–200 nm, followed by a linear increase in Al content through the first micrometer of material, where it comes to a maximum; then the concentration decreases to form an Al-poor core.[22,23] These results point to the highly complex, inhomogeneous nature of the material from both a structural and compositional perspective, and indicate a non-uniform distribution of acid sites.[22] Therefore, the analyzed cross-section was carefully selected to probe distinct subunits. Also, it needs to be emphasized that the size of the analyzed needles is approximately three orders of magnitude smaller than the crystal, providing "nano-snapshots" of the material at distinct locations.

Figure 2a shows the bulk Si/Al ratio as well as the coke content of each needle harvested from the ZSM-5 crystal, measured by APT (see the Supporting Information for a discussion of the Si/Al ratios). The variations observed in the Si/Al ratios between needles harvested from distinct regions of the cross-section are consistent with the known variation in Si/Al ratio qualitatively depicted in Figure 1c. The complete composition determined for each needle can be found in Table S1. As Figure 2a clearly shows, there is a strong correlation between the amount of coke and the Si/Al ratio, which determines the density of Brønsted acid sites; the location of the needle also correlates with both the Si/Al ratio and coke content. The small amount of material measured per APT needle (tens to hundreds of thousands of cubic nanometers), makes this correlation especially meaningful, as needles that are from similar positions on the microscale have different Al concentrations. Additionally, for needles 1 and 2, which have similar Si/Al ratios, similar coke (^{13}C) contents were found, underscoring the relationship between Si/Al ratio and carbon deposit formation. The ^{13}C concentrations are consistent with the expected trend as they are highest near the surface and decrease towards the center of the crystal.

One of the most important features of APT is that it gives the ability to reconstruct the 3D atomic composition of the analyzed volume. The 3D reconstruction of needle 3 is shown in Figure 1e for all elements, and Figure 1f for ^{13}C; full compositional reconstructions of all APT needles are provided in Figure S4. Visually, needles 2 and 3 exhibit inhomogenities that span tens of nanometers, while the other needles appear to be homogeneous across all elements. Isosurface analysis was used to quantitatively identify inhomogeneous areas in needles 2 and 3 (details about isosurface analysis can be found in the Supporting Information). The ^{13}C isosurface identified in needle 3 is shown along with a compositional histogram in Figure 2b (a larger view is given in Figure S5), defined by a 3% ^{13}C boundary (one side of the surface contains > 3% ^{13}C and the other side less than this, see the Supporting Information for a discussion of the isosurface boundary).[19,24] This isosurface highlights a region with an abrupt change from a very low ^{13}C
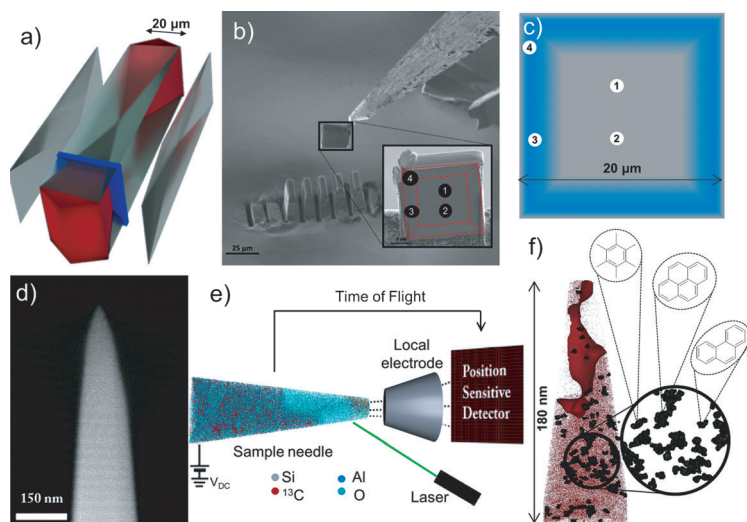

Figure 1. a) Expanded view 3D schematic of a large ZSM-5 crystal showing the internal architecture of the material which is composed of several distinct subunits,[22] as well as the location of the removed cross-section (blue panel) prepared by FIB milling. b) The cross-section that was removed for APT needle preparation. The red dashed lines show the locations of the subunits and the black numbered circles indicate the needle locations. c) Schematic representation of Al zoning in the ZSM-5 cross-section; blue represents regions with higher Al content and approximate needle positions are numbered 1 to 4. d) SEM image of needle 3 as prepared by FIB milling before APT analysis. e) A schematic overview of the APT technique showing the 3D distribution of all ions (Al, O, Si, and ^{13}C) as detected in needle 3. f) Reconstruction for ^{13}C (red) distribution in needle 3 together with a 3% ^{13}C concentration isosurface identified on the basis of those distributions and identified ^{13}C clusters (black overlay). Corresponding changes in local atom concentrations across the isosurface are reported in Figure 2b. The magnified region shows the distribution of ^{13}C clusters only (each dot represents one ^{13}C ion in the ^{13}C cluster). The molecules indicated are possible coke species that are consistent with median ^{13}C cluster sizes, though APT cannot provide molecular fingerprinting. The ZSM-5 crystal, cross-section, and needle shown are the actual samples discussed in the manuscript and were used in the MTH reaction with ^{13}C-labeled methanol for 90 min at 623 K.
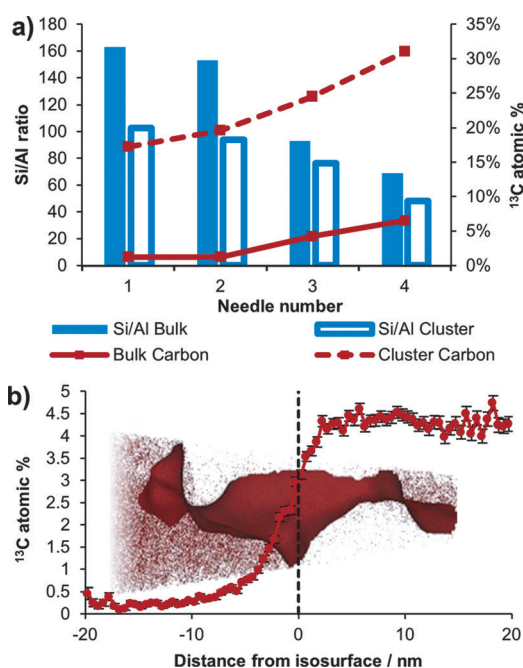
Figure 2. a) Bulk and cluster Si/Al ratio and ^{13}C atomic % plotted for APT needles 1 to 4 (see the Supporting Information for a discussion of the quantification of the Si/Al ratio). Clusters are defined as groups of closely spaced ^{13}C atoms and the cluster Si/Al ratio is inside the volume occupied by the clusters, averaged over all clusters in each needle. b) Compositional histogram across the ^{13}C isosurface in needle 3 (3 % boundary; only a selected portion of needle 3 is shown).

Figure 3. a) Map of ^{13}C clusters identified in APT needle 3 superimposed over all ^{13}C ions. The large black dots represent the ^{13}C cluster atoms and the smaller red dots represent all ^{13}C ions. b) NNDs for ^{13}C in needle 3 along with Gaussian fits of the data. The measured data is plotted in red and randomized data in black. The ^{13}C solute distribution is best described by two Gaussians (dashed lines), indicating the presence of a population of clusters with smaller NNDs than those found for the remaining atoms or the randomized data. c) NNDs for Al in needle 3 showing an unimodal distribution, that is, the absence of any Al clusters. d) Radial distribution function for needle 3, which describes the normalized radial concentration of Al and Si relative to the bulk starting at the center of the ^{13}C cluster. The short-distance error bars are large because of the low number of ions measured close to the center of the cluster.

content, less than 0.5 % ^{13}C, to a region with nearly 5 % ^{13}C. The reasons behind this rapid change in coke content are not obvious as the proximity histogram in Figure S6 shows there is not a significant change in Si/Al ratio near the abrupt increase in carbon content. Likely it is related to some structural features that cannot be resolved using the APT technique, such as a boundary between subunits or a crystallographic defect. Additional ^{13}C isosurfaces were identified in needles 2 and 3 (Figures S7 to S10), also without a significant correlation with the Si/Al ratio.

The true power of the APT technique to study zeolite crystals and monitor the formation of coke comes from the cluster analysis, as explained in-depth in the Supporting Information. Clusters are compositional inhomogeneities too small to be identified using isosurface analysis. One method of determining if statistically significant clusters exist is a comparison of the nearest neighbor distances (NNDs) of the collected and randomized data, as exemplified in Figures 3 b,c for ^{13}C and Al in needle 3 (carbon poor areas were not analyzed, shown in Figures S11 and S12, NNDs for all needles are in Figures S13 and S14). Additionally, the frequency distribution analysis (FDA) for ^{13}C and Al in each needle is given in Table S2. The evaluation of both the NNDs and the FDA for ^{13}C and Al reveals that statistically significant ^{13}C clusters exist in needles 1–4. Table S3 reports the number of ^{13}C clusters found per needle, the average cluster size, the compositions of the clusters for needles 1–4, and the parameters N_{min} and D_{max}, used to define the clusters. A map of the
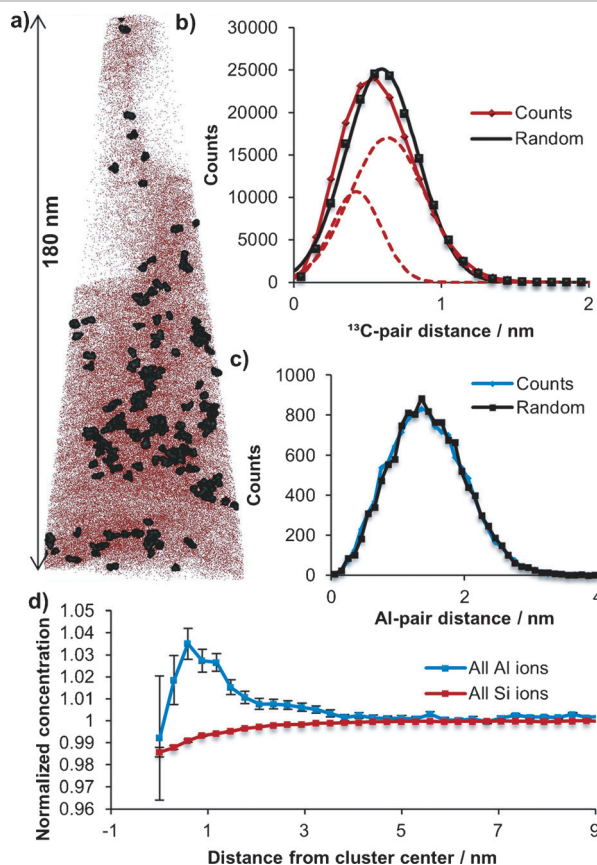
^{13}C clusters identified in needle 3 is displayed in Figure 3 a superimposed over all ^{13}C ions.

Because the FDA showed that the ^{13}C atoms contained a population with NNDs that were significantly shorter than a random distribution in needles 1–4, each NND was fit with two Gaussians and compared to a randomized data set. The centers of the distributions for the actual and randomized data are given in Table S4. In needles with clusters, the measured distribution is excellently described using two Gaussians. Interestingly, one Gaussian is centered near the maximum of the randomized NND distribution, while the second Gaussian is centered at a much lower atom pair distance. These two populations of ^{13}C NNDs indicate that these needles contain clusters of ^{13}C atoms with a dense packing of atoms, as well as a population of ^{13}C atoms with a random distribution.

A wide range of cluster sizes was identified in the needles (Table S3) and the smallest statistically relevant clusters contained 10 ^{13}C atoms. As the APT instrument used in this work has an ion detection efficiency of approximately 37% (equal for all ions), these pockets of coke contain approximately 30 carbon atoms. Figure S15 shows potential coke species known to exist in ZSM-5.[12,25] Based on these species, the smallest clusters can contain 1–2 molecules. The median detected cluster sizes of 36–69 carbon atoms (after accounting for instrument efficiency) indicate most clusters can contain several occluded aromatic species. It should be emphasized here that the APT technique is unable to provide molecular fingerprinting information of the ^{13}C clusters detected.

When the range of sizes of the ^{13}C clusters is considered in conjunction with the ^{13}C isosurface analysis, insight can be gathered into the coke formation mechanism. The smallest clusters found are likely the first to be formed. These small ^{13}C clusters then grow in size into the larger clusters observed. Finally, they merge to form the coke-rich regions identified using isosurface analysis. This is consistent with previously proposed coke formation mechanisms: At the beginning of the reaction methanol will be present throughout the zeolite crystals, which is why we see ^{13}C clusters in all needles; then as the reaction proceeds and the material deactivates, the coke will be present in greater quantity at the crystal surface, reflected by the higher coke contents we found in the needles taken from regions near the crystal's surface.[7–13]

A closer examination of the relationship between ^{13}C clusters and Al content was conducted using the radial distribution function (RDF, discussed in the Supporting Information) with ^{13}C cluster centers. In needles 1 and 2 a pronounced affinity was found for Al to be in the clusters compared to the bulk, with a much higher normalized Al concentration in the clusters (see Figure S16). In needle 3, the normalized Al concentration was also significantly higher around ^{13}C cluster centers than within the bulk, shown in Figure 3d. The RDF is a clear indication that the coke clusters form preferentially around areas with elevated Al content, while the normalized Al content approaches unity away from the center of the ^{13}C clusters. The correlation between the clusters and Al content is also reflected in a comparison between the bulk and cluster Si/Al ratio, shown in Figure 2a, highlighting the increased density of Al atoms (Brønsted acid sites) within the clusters.

The same analyses used to reveal the ^{13}C clusters were also applied to the measured Al distributions, but no inhomogenities could be identified. While it seems counterintuitive that a significant increase in Al concentration within the clusters was found, but no Al clusters were observed, this can be explained by considering that the ^{13}C content in the clusters increased at least five-fold compared to the bulk, which allowed clusters to be identified, while the Al increase was much smaller, preventing statistically relevant Al clusters from being identified.

APT has revealed the existence of small clusters of coke atoms in a ZSM-5 crystal that was partially deactivated in the ^{13}C labeled MTH reaction. These ^{13}C clusters correlate with regions of locally decreased Si/Al ratio, that is, an increase of Brønsted acid site density on a nanoscopic level, and are likely the first coke precursors to be formed in the material, which can lead to pore blockage and subsequent catalyst deactivation. This study shows the importance of controlling zeolite acid site density on the nanoscale as a means to control coke formation. It also shows that the first coke precursor species can form throughout the material and are related to nanoscopic and minute differences in Al content. This successful application of APT to coked zeolites demonstrates the technique is capable of probing nonconductive, inhomogeneous catalytic materials, and has the potential to be applied to numerous other systems.

[1] E. T. C. Vogt, G. T. Whiting, A. D. Chowdhury, B. M. Weckhuysen, *Adv. Catal.* **2015**, 143.

[2] W. Vermeiren, J.-P. Gilson, *Top. Catal.* **2009**, *52*, 1131.

[3] A. M. Beale, F. Gao, I. Lezcano-Gonzalez, C. H. F. Peden, J. Szanyi, *Chem. Soc. Rev.* **2015**, *44*, 7371.

[4] S. Brandenberger, O. Kröcher, A. Tissler, R. Althoff, *Catal. Rev.* **2008**, *50*, 492.

[5] U. Olsbye, S. Svelle, M. Bjørgen, P. Beato, T. V. W. Janssens, F. Joensen, S. Bordiga, K. P. Lillerud, *Angew. Chem. Int. Ed.* **2012**, *51*, 5810; *Angew. Chem.* **2012**, *124*, 5910.

[6] U. Olsbye, S. Svelle, K. P. Lillerud, Z. H. Wei, Y. Y. Chen, J. F. Li, J. G. Wang, W. B. Fan, *Chem. Soc. Rev.* **2015**, *44*, 7155.

[7] D. M. Bibby, N. B. Milestone, J. E. Patterson, L. P. Aldridge, *J. Catal.* **1986**, *97*, 493.

[8] B. A. Sexton, A. E. Hughes, D. M. Bibby, *J. Catal.* **1988**, *109*, 126.

[9] F. L. Bleken, K. Barbera, F. Bonino, U. Olsbye, K. P. Lillerud, S. Bordiga, P. Beato, T. V. W. Janssens, S. Svelle, *J. Catal.* **2013**, *307*, 62.

[10] D. Mores, E. Stavitski, M. H. F. Kox, J. Kornatowski, U. Olsbye, B. M. Weckhuysen, *Chem. Eur. J.* **2008**, *14*, 11320.

[11] L. R. Aramburo, S. Teketel, S. Svelle, S. R. Bare, B. Arstad, H. W. Zandbergen, U. Olsbye, F. M. F. de Groot, B. M. Weckhuysen, *J. Catal.* **2013**, *307*, 185.

[12] R. Y. Brogaard, B. M. Weckhuysen, J. K. Nørskov, *J. Catal.* **2013**, *300*, 235.

[13] J. P. Hofmann, D. Mores, L. R. Aramburo, S. Teketel, M. Rohnke, J. Janek, U. Olsbye, B. M. Weckhuysen, *Chem. Eur. J.* **2013**, *19*, 8533.

[14] D. Mores, J. Kornatowski, U. Olsbye, B. M. Weckhuysen, *Chem. Eur. J.* **2011**, *17*, 2874.

[15] L. R. Aramburo, E. De Smit, B. Arstad, M. M. Van Schooneveld, L. Sommer, A. Juhin, T. Yokosawa, H. W. Zandbergen, U. Olsbye, F. M. F. De Groot, B. M. Weckhuysen, *Angew. Chem. Int. Ed.* **2012**, *51*, 3616; *Angew. Chem.* **2012**, *124*, 3676.

[16] D. J. Larson, T. J. Prosa, R. M. Ulfig, B. P. Geiser, T. F. Kelly, *Local Electrode Atom Probe Tomography*, Springer, New York, **2013**.

[17] M. K. Miller, T. F. Kelly, K. Rajan, S. P. Ringer, *Mater. Today* **2012**, *15*, 158.

[18] B. Gault, M. P. Moody, J. M. Cairney, S. P. Ringer, *Mater. Today* **2012**, *15*, 2.

[19] M. K. Miller, R. G. Forbes, *Mater. Charact.* **2009**, *60*, 461.

[20] G. Möbus, B. J. Inkson, *Mater. Today* **2007**, *10*, 18.

[21] D. E. Perea, I. Arslan, J. Liu, Z. Ristanović, L. Kovarik, B. W. Arey, J. A. Lercher, S. R. Bare, B. M. Weckhuysen, *Nat. Commun.* **2015**, *6*, 7589.

[22] L. Karwacki, M. H. F. Kox, D. A. M. de Winter, M. R. Drury, J. D. Meeldijk, E. Stavitski, W. Schmidt, M. Mertens, P. Cubillas, N. John, A. Chan, N. Kahn, S. R. Bare, M. Anderson, J. Kornatowski, B. M. Weckhuysen, *Nat. Mater.* **2009**, *8*, 959.

[23] Z. Ristanović, J. P. Hofmann, U. Deka, T. U. Schülli, M. Rohnke, A. M. Beale, B. M. Weckhuysen, *Angew. Chem. Int. Ed.* **2013**, *52*, 13382; *Angew. Chem.* **2013**, *125*, 13624.

[24] O. C. Hellman, J. A. Vandenbroucke, J. Rüsing, D. Isheim, D. N. Seidman, *Microsc. Microanal.* **2000**, *6*, 437.

[25] I. Yarulina, J. Goetze, C. Gücüyener, L. van Thiel, A. Dikhtiarenko, J. Ruiz-Martinez, B. M. Weckhuysen, J. Gascon, F. Kapteijn, *Catal. Sci. Technol.* **2016**, *6*, 2663.